Journal of Inflammation Research Dovepress

Open Access Full Text Article ORIGINAL RESEARCH

Mechanism of Qingdai in Alleviating Acute Lung Injury by Inhibiting the JAK2/STAT3 Signaling Pathway

Lu Qi[1–3,*], Shun Wang[1,3,*], Tao Guo[1,3], Zhuocao Qi[1,3], Suwan Wu[1,3], Dan Gao[1,3], Zhiqiang Yan[4], Bo Tan[4], Aidong Yang[1,3]

[1]The Research Center for Traditional Chinese Medicine, Shanghai Institute of Infectious Diseases and Biosecurity, Shanghai University of Traditional Chinese Medicine, Shanghai, 201203, People's Republic of China; [2]The First College of Clinical Medical Science, China Three Gorges University & Yichang Central People's Hospital, Yichang, 443003, People's Republic of China; [3]School of Traditional Chinese Medicine, Shanghai University of Traditional Chinese Medicine, Shanghai, 201203, People's Republic of China; [4]Laboratory of Clinical Pharmacokinetics, Shuguang Hospital Affiliated to Shanghai University of Traditional Chinese Medicine, Shanghai, 201203, People's Republic of China

*These authors contributed equally to this work

Correspondence: Aidong Yang; Bo Tan, Email aidongy@126.com; tbot@163.com

Objective: Qingdai (QD) is a traditional Chinese medicine (TCM) commonly used in clinical practice to treat acute lung injury/acute respiratory distress syndrome (ALI/ARDS). However, the mechanisms underlying the effects of QD remain not fully understood. This investigation demonstrated QD alleviated LPS-induced ALI in mice and exerted anti-inflammatory effects by inhibiting the JAK2/STAT3 signaling pathway.

Methods: The active compounds of QD were identified through UPLC-LTQ-Orbitrap-MS/MS. Network pharmacology predicted potential pharmacological targets and the signaling pathways contributed to the effectiveness of QD in treating ALI. Molecular docking assessed the binding of active components to critical targets. ALI mice triggered by Lipopolysaccharides (LPS) were used for transcriptomic analysis to assess alterations in pulmonary gene expression. The pathological changes of lung tissue were analyzed via HE staining. Proinflammatory cytokine levels in serum were measured using ELISA, and the mRNA expression was measured by RT-qPCR. Western blot analysis evaluated protein expression related to the JAK2/STAT3 signaling pathway. Additionally, RAW264.7 cells induced by LPS were treated with QD to measure proinflammatory cytokines and JAK2/STAT3 signaling pathway protein expression.

Results: Six major components of QD were identified. Network pharmacology predicted JAK2 and STAT3 as targets for QD in ALI treatment, with KEGG analysis highlighting the JAK/STAT signaling pathway. Transcriptomics confirmed the JAK/STAT signaling pathway in the therapeutic effects of QD. Molecular docking demonstrated high binding affinities of bisindigotin, isoindigo, and 6-(3-oxoindolin-2-ylidene)indolo[2,1-b]quinazolin-12-one (IQO) to JAK2 and STAT3. In vivo, QD reduced lung inflammation, downregulated proinflammatory cytokines, and inhibited JAK2/STAT3 signaling pathway. In vitro, QD mitigated LPS-triggered inflammatory responses in RAW264.7 macrophages by inhibiting the same pathway.

Conclusion: The therapeutic effects of QD in ALI might be mediated by the modulation of the JAK2/STAT3 signaling pathway, which may make it a valuable therapeutic strategy for ALI/ARDS.

Keywords: Qingdai, acute lung injury, anti-inflammation, macrophages, JAK2/STAT3

Introduction

Acute lung injury or acute respiratory distress syndrome (ALI/ARDS) represents severe pulmonary afflictions characterized by intense inflammation and cytokine release, frequently triggered by severe infections, trauma, or sepsis. The pathophysiological processes in ALI/ARDS involve an exaggerated inflammatory reaction and pulmonary edema, which stem from the disruption of the alveolar-capillary barrier.[1] These conditions are associated with high mortality rates, which increase significantly with age; for example, patients over 85 years of age face a mortality rate of around 60%.[2,3]

Received: 27 September 2024
Accepted: 14 December 2024
Published: 21 December 2024

Graphical Abstract

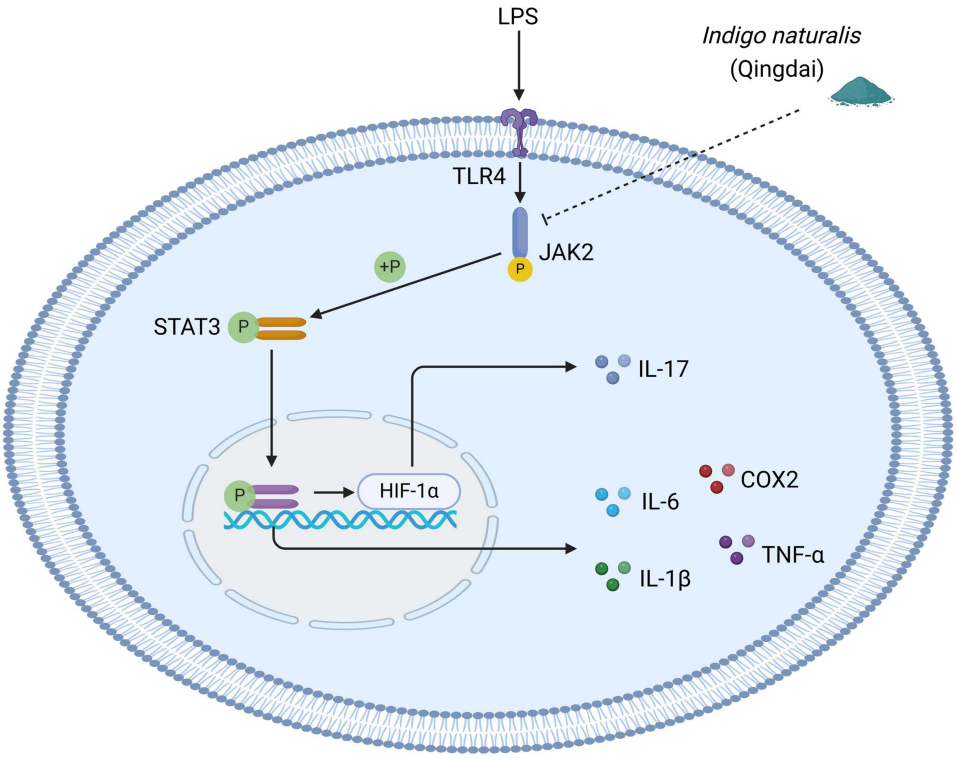

Despite advances in clinical and experimental research, current therapeutic strategies for ALI/ARDS remain inadequate, with patients often suffering long-term impairments that adversely affect their quality of life.[4] This highlights the pressing requirement for innovative and efficacious therapeutic approaches.

Traditional Chinese Medicine (TCM) has a rich historical background and is a significant component of clinical practice in East Asia, especially for managing respiratory conditions. TCM provides alternative and complementary methods for managing pulmonary conditions, including pneumonia, chronic obstructive pulmonary disease (COPD), and pulmonary fibrosis.[5] Its efficacy in alleviating symptoms and enhancing physiological function in ALI is well-documented and has a proven safety record.[6] *Indigo naturalis*, known as Qingdai (QD) in TCM, is obtained from the desiccated stems or foliage of certain plants, including *Baphicacanthus cusia* (Nees) *Bremek, Isatis indigotica*, and *Fort Polygonum tinctorium Ait*. It is renowned for its heat-clearing, detoxifying, and expectorant properties and is used in treating upper respiratory tract infections, bronchitis, and pneumonia.[7] Additionally, QD is a central component in TCM for treating pulmonary atrophy, which corresponds to pulmonary fibrosis in the later stages of ALI, demonstrating both efficacy and safety in clinical settings.[8]

Recent pharmacological research has underscored various activities of QD, including antioxidant, antiviral, antibacterial, immunomodulatory, and anticancer properties.[9] Particularly, its anti-inflammatory and anti-pyroptotic capabilities are of notable importance.[10,11] Clinical research shows the efficacy of QD in treating ulcerative colitis (UC), possibly through the suppression of the TLR4/MyD88/NF-κB signaling pathway.[12] Indirubin, an active compound in QD, offers protective effects in osteoarthritis by targeting IL-1β-induced MAPK and NF-κB pathways,[13] as well as in pulmonary fibrosis by dampening the TGF-β/Smad signaling pathway.[14] Additionally, QD mitigates influenza virus-induced ALI in mice through its antiviral, antioxidant, and anti-inflammatory properties.[15]

Given the historical importance of QD in TCM and growing evidence of its therapeutic potential, we aimed to investigate its bioactive constituents and potential mechanisms through which it regulates ALI. The study utilizes high-

resolution mass spectrometry, network pharmacology, molecular docking, and transcriptomics to elucidate the effects of QD. Subsequent experiments in mouse and cell models validated how QD alleviated ALI, with a focus on the JAK2/STAT3 signaling pathway.

Materials and Methods

Reagents

Lipopolysaccharide (LPS, L2880) was obtained from Sigma-Aldrich (St. Louis, MO). *Indigo naturalis* (QD, 220103) was sourced from Hubei Tianji Pharmaceutical Co., Ltd. (Hubei, China) and authenticated by Professor Zhiying Dong (Shanghai University of Traditional Chinese Medicine, China), which was deposited in Hubei Provincial Hospital of Traditional Chinese Medicine. Dexamethasone (501220321) was acquired from Xinyi Jinjian Pharmaceutical Co., Ltd. (Tianjin, China).

For antibody detection, the following antibodies were used: Anti-JAK2 (3230, 1:1000), Anti-p-JAK2 (4406, 1:1000), Anti-STAT3 (12640, 1:1000), Anti-p-STAT3 (9145, 1:2000), and Anti-COX2 (12282, 1:1000), all purchased from Cell Signaling Technology (Danvers, MA). Anti-HIF-1α (1:1000, ab179483) was obtained from Abcam (Cambridge, UK). Anti-IL17A (ER1902-37, 1:500) was acquired from Huabio (Hangzhou, China). Anti-GAPDH (AG0919-1, 1:5000) and goat anti-rabbit IgG (H+L) conjugated with HRP (A0208) were purchased from Beyotime Biotechnology (Shanghai, China).

Preparation of QD Lyophilized Powder

One kilogram of *Indigo naturalis* (Qingdai, QD), obtained from the desiccated stems or foliage of *Baphicacanthus cusia* (Nees) *Bremek, Isatis indigotica Fort*., and *Polygonum tinctorium Ait*, was wrapped in eight layers of gauze and soaked in deionized water for 20 minutes. Then, bring it to a boil, collect the filtrate after 30 minutes, and repeat the process twice. The combined extracts were concentrated into 500mL and freeze-dried in a freeze-drying machine (Christ, Germany), resulting in 22.6 g of lyophilized QD powder.

Identification of Chemical Components in Lyophilized Powder

A 50 mg of lyophilized QD water extract powder was dissolved in 800 μL of methanol, then vortexed and ultrasonicated for 15 minutes. After centrifugation and filtration, the liquid was analyzed by UPLC-LTQ-Orbitrap-MS/MS, which includes the ACQUITY UPLC (Waters) and the Orbitrap Elite ion trap mass spectrometer (Thermo Fisher, Germany). The chromatographic resolution was achieved using an HSS T3 column (Waters, 100 mm × 2.1 mm, 1.8 μm) with a gradient elution program, starting at 2% B for 0 minutes, increasing to 2% B at 0.5 minutes, to 5% B by 2 minutes, to 15% B by 3 minutes, to 50% B by 13 minutes, to 95% B by 25 minutes, holding at 95% B for 5 minutes until 30 minutes, then re-equilibrating to 5% B by 30.5 minutes, and maintaining at 5% B until 35 minutes. Mass spectrometry utilized an electrospray ionization (ESI) source in positive and negative ionization modes. Data processing was carried out with Compound Discoverer 3.3 software (Thermo Fisher), using the natural products template to match and identify compounds against the Otcml database (Thermo Fisher).

Network Pharmacology Experiments

Uncovering Active Compounds and Their Molecular Targets in QD

The active compounds and their respective targets of QD were ascertained utilizing the Traditional Chinese Medicine Systems Pharmacology Database and Analysis Platform (TCMSP, http://tcmspw.com/tcmsp.php),[16] the Traditional Chinese Medicine Integrated Database (TCMID, http://www.megabionet.org/tcmid), and relevant published literature.[17,18] The selection criteria were established to include a minimum oral bioavailability (OB) of 30% and a drug-likeness (DL) score exceeding 0.18.

Construction of Compound-Target Network and PPI Network

Disease-related targets for ALI and ARDS were determined by searching the OMIM (https://www.omim.org/) and GeneCard (https://www.genecards.org/) databases using these keywords. The disease targets were combined to create a union set. Active compound and disease targets were intersected using the Venn diagram package in R software (V

4.2.2). Network text files were created with Perl 5.32.1 and visualized in Cytoscape 3.10.0 to analyze the pharmacological network of QD and ALI. Intersecting targets were uploaded to the STRING database (https://string-db.org/) with a confidence score threshold of 0.4, utilizing human gene datasets to construct a protein-protein interaction (PPI) network. The network visualization and analysis were performed using the Cytoscape software, supplemented with the CytoNCA plugin for topological examination.

Analyses of Gene Enrichment and Pathway

The functional enrichment analysis of GO terms and a KEGG pathway analysis were conducted on the intersecting genes between drug and disease targets using the R language (V4.2.2) through the Bioconductor platform (https://www.bioconductor.org/). This analysis utilized the Colorspace, Stringi, DOSE, ClusterProfiler, and Pathview packages. The top 30 ranked entries were subsequently visualized.

Molecular Docking

Molecular docking was conducted using AutoDock Vina (Center for Computational Structural Biology, V4.2.6), and the interactions between the core targets of interest and the primary active components of QD were assessed. These components were identified through network pharmacology and UPLC-LTQ-Orbitrap-MS/MS.

Preparation of Receptors and Ligands

The three-dimensional structures of the receptors were sourced from the Protein Data Bank (https://www.rcsb.org/) and stored in PDB format, while the ligands were retrieved from the TCMSP (https://old.tcmsp-e.com/tcmsp.php) and saved in mol2 format. The AutoDockTools was employed to add hydrogen atoms and charges, saving the receptors as pdbqt files. Ligands were also converted to pdbqt format using AutoDockTools (Center for Computational Structural Biology, V4.2.6).

Setting the Receptor's Binding Pocket

The receptor was opened in AutoDockTools 4.2.6 (Center for Computational Structural Biology, V4.2.6), and a box was set up to encompass the binding pocket. The corresponding values for center_x, center_y, center_z, size_x, size_y, and size_z were set based on the box size. Num_modes was set to 20, energy_range to 5, and exhaustiveness to 64.

Molecular Docking and Visualization

Molecular docking and conformational analysis were conducted by AutoDock Vina (Center for Computational Structural Biology, V4.2.6), with the calculation of binding affinities. The molecule with the strongest affinity was selected, and its best conformation was saved for further analysis of hydrogen bonds and receptor-ligand interactions. Visualization was conducted using Pymol software (Schrodinger, V.2.6) and Ligplus (EMBL-EBI, V.2.2).

Animal Grouping and Treatment

The mice were accommodated in an environment maintained at a temperature of 20–26°C, with humidity levels ranging from 40% to 70%, and subjected to a 12-hour alternating light/dark cycle. After acclimatization, the animals were assigned randomly to six distinct groups for subsequent experiment (n = 12 per group): Control, LPS, Dexamethasone (DEX, 5 mg/kg), low dose of QD (QD-L, 0.195 g/kg), medium dose of QD (QD-M, 0.39 g/kg), and high dose of QD (QD-H, 0.78 g/kg). Doses were adjusted based on human-animal body surface area conversions.[19] The QD and DEX groups were given the corresponding drugs by gavage for 7 days. The Control group received saline. One hour after the last oral administration, the LPS, QD, and DEX groups were intratracheally instilled with LPS (5 mg/kg, 50 μL) to induce the model as previously reported.[20,21] The Control group received saline. The mice were euthanized 24 hours following the administration, after which blood serum and lung tissue samples were retrieved.

Hematoxylin and Eosin (HE) Staining

The left inferior lung lobe was fixed with 4% paraformaldehyde. After staining with HE, the slides were analyzed using a pathology slide scanner (WS-10, Zhiyue Medical Technology Co., Ltd., Jiangsu, China). Pathological scoring followed the previous method.[22] Three separate pathologists, unaware of the group allocations, assessed the HE-stained slides with

three samples per group. The severity of edema, atelectasis, necrosis, inflammation, hemorrhage, and hyaline membrane formation was rated from 0 (no injury) to 4 (100% injury) in three randomly selected areas per image (200× magnification).

Transcriptomic Analysis

mRNA was extracted from mouse lung tissues in the control, LPS-induced ALI, and QD treatment groups using the MJZol Total RNA Extraction Kit (Majorbio Bio-Pharm, Shanghai, China), followed by purification with the RNA Purification Kit (Biowest, Spain). Sequencing libraries were prepared with the Stranded mRNA Prep Ligation Kit (Illumina, NY). This process involved extracting total RNA, enriching mRNA with Oligo dT, fragmenting it, reverse transcribing to synthesize cDNA, ligating adaptors, selecting fragments, and finally sequencing on the NovaSeq X Plus platform (Illumina, San Diego, CA).

Cell Culture

The RAW264.7 cells, obtained from the Cell Bank of Chinese Academy of Sciences, were cultivated in Dulbecco's Modified Eagle Medium (DMEM) supplemented with Fetal Bovine Serum (FBS, 10%), penicillin (1%), and streptomycin (1%). The cells were kept at 37°C in an incubator with a 5% CO_2 atmosphere. Following the evaluation of cell viability through the CCK8 assay, QD was applied at three distinct concentrations: a low dose of 50 μg/mL, a medium dose of 100 μg/mL, and a high dose of 200 μg/mL. Cells were incubated for 24 hours with different concentrations of QD and LPS at a concentration of 1ug/mL, as indicated by a previous study.[21]

Cell Proliferation Assay

RAW264.7 cells cultured in the logarithmic growth phase were diluted and seeded into a 96-well plate at a rate of 7000 cells per well. Post adhesion period, the cells were treated with various concentrations of the drug for 24 hours. Cell viability was then assessed using a CCK8 solution (Beyotime Biotechnology, Shanghai, China).

Elisa

Serum from mice and supernatants from RAW264.7 cells were collected, and the concentrations of IL-1β, IL-6, TNF-α, and IL-17 were determined utilizing Enzyme-Linked Immunosorbent Assay (ELISA) kits from Boyan Biotechnology (Nanjing, China).

RT-qPCR

Total RNA was extracted from treated RAW264.7 cells and lung tissue using the EZ-press RNA Purification Kit (B0004D, Suzhou, China). The isolated RNA was converted to cDNA using the PrimeScript™ Reverse Transcription Master Mix (RR036A, Takara, Japan). Quantitative PCR (qPCR) was performed using the TB Green® Premix Ex Taq (RR420A, Takara, Japan) on a real-time PCR instrument (QuantStudio3, ABI, USA). The primer sequences are provided in Supplementary Table 1 and were synthesized by Sangon Biotech (Shanghai, China). GAPDH mRNA expression was used as an internal control for semi-quantitative analysis.

Western Blot

Protein extraction was carried out from both cellular and pulmonary samples utilizing RIPA buffer (P0013B, Beyotime). An overnight incubation of the primary antibody was performed after electrophoresis and transfer, followed by an incubation at room temperature of the secondary antibody (1:5000) for one hour. A chemiluminescent substrate was added, and the signal was detected using a FlourChem E imaging system (ProteinSimple, San Jose, CA).

Statistical Analysis

Each experimental procedure was repeated thrice, with results presented as the mean ± standard deviation (SD). Statistical evaluations were executed with the SPSS package version 22 (IBM, Armonk, NY). One-way ANOVA for comparisons between multiple groups must be verified for homogeneity of variance, and *t*-tests were applied for comparisons between two groups. A p-value of less than 0.05 was taken to indicate statistical significance. The graphical representations were generated using GraphPad Prism (Version 8, San Diego, CA).

Results

Analysis of Major Active Components of QD

Using UPLC-LTQ-Orbitrap-MS/MS, the mass spectra were correlated with entries in the Otcml database (Table 1, Figure 1). Six compounds with strong responses in the positive ion mode and the values of mzCloud Best Match ≥ 85 were identified: Nicotinic acid, Adenosine, L-Phenylalanine, Indigo, Indirubin, and α-Linolenic acid.

QD Alleviated Inflammation in the Lung Tissue of Mice with ALI

HE staining showed that the lung tissue in the control group had clear alveolar structures and intact airway epithelium with no pathological changes. In contrast, LPS treatment caused disordered lung tissue with numerous red blood cells in the alveolar spaces, hemorrhage patches, thickened alveolar walls, hyaline membrane formation, and epithelial cell detachment with neutrophil and lymphocyte infiltration. The QD and DEX could diminish these pathological alterations (Figures 2A-2B). ELISA results revealed elevated concentrations of IL-1β, IL-6, TNF-α, and IL-17 in the LPS group as opposed to the control group, with QD significantly lowering the levels of these cytokines (Figure 2C). RT-qPCR further showed that QD decreased mRNA expression of IL-1β, IL-6, and TNF-α in the lung tissue of ALI mice (Figure 2D).

Network Pharmacology Analysis

After querying the TCMSP and TCMID databases, nine active compounds were identified (see Supplementary Table 2). Drug targets were retrieved, revealing that these compounds targeted 56 unique proteins, excluding bisindigotin, which had no identified targets. A total of 10,550 ALI-related targets were found via GeneCards and OMIM. Intersection analysis identified 55 common targets. A pharmacological network was created using Cytoscape 3.10.0, featuring 65 nodes (eight compounds, 55 targets) and 141 edges (Figure 3A). Topological analysis with CytoNCA provided Degree, Eigenvector, Betweenness, and Closeness values (Supplementary Table 3).

A Protein-Protein Interaction (PPI) network was assembled using STRING, with the extraction of the core network depicted (Figure 3B). The top 30 targets were ranked and visualized in R, with JAK2 and STAT3 among the top ten (Figure 3C). GO analysis identified 1060 biological processes, highlighting significant ones like "response to lipopolysaccharide" (Figure 3D). KEGG analysis found 126 pathways, including JAK/STAT and IL-17 pathways, with the top 30 pathways visualized (Figure 3E).

Molecular Docking Analysis

Molecular docking predicted the binding modes and affinities of the active components with JAK2 and STAT3. The minimum binding energies are listed in Supplementary Table 4. The three active components with the strongest affinities were selected for detailed analysis of hydrogen bonding and receptor-ligand interactions with JAK2 (PDB ID: 8c09) and STAT3 (PDB ID: 6njs). The chemical structures of bisindigotin, isoindigo, and IQO are shown in Figure 4A. These compounds were found to bind closely with JAK2 and STAT3. Bisindigotin formed a hydrogen bond with Lys677(A) of JAK2 (Figure 4B) and hydrophobic interactions with Asp566(A), Arg335(A), and Asp570(A) of STAT3 (Figure 4E). Isoindigo interacted with Val629(A) of JAK2 through a hydrogen bond (Figure 4C) and with Asp570(A), Asp566(A),

Table 1 Active Compounds Identified in QD by UPLC-LTQ-Orbitrap-MS/MS

No.	RT (min)	Name	Formula	Determined MW (Da)	m/z Cloud*	MS (m/z)	MS^2 (m/z)
1	1.5	Nicotinic acid	C6H5NO2	123.03176	96.8	124.04	136.06,214.09
2	2.5	Adenosine	C10H13N5O4	267.09648	100	268.10	160.08,216.09,189.19
3	4.1	L-Phenylalanine	C9H11NO2	165.07865	89.7	166.09	413.27
4	15.6	Indigo	C16H10N2O2	262.07396	95.5	263.08	337.23
5	16.2	Indirubin	C16H10N2O2	262.07387	98.8	263.08	263.08,214.09,100.11
6	19.4	α-Linolenic acid	C18H30O2	278.22399	99.0	279.23	149.02,284.33,400.25

Note: m/z Cloud*denote the values of mzCloud Best Match.

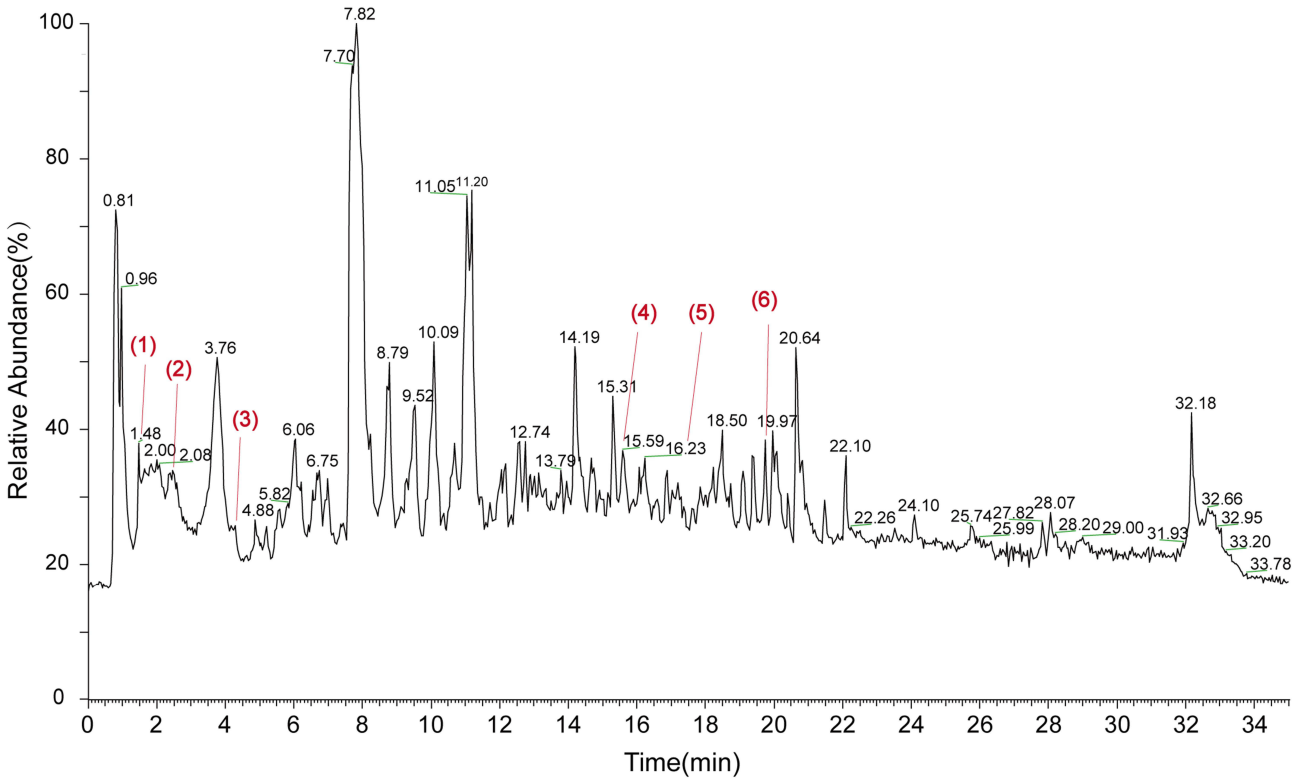

Figure 1 Positive Ion Chromatogram of Qingdai by UPLC-LTQ-Orbitrap-MS/MS. Each labeled peak represents an identified compound: (1) Nicotinic acid; (2) Adenosine; (3) L-Phenylalanine; (4) Indigo; (5) Indirubin; (6) α-Linolenic acid.

and His332(A) of STAT3 (Figure 4F). IQO established hydrogen bonding with the Ser633 residue in JAK2 (Figure 4D) and the Leu438 residue in STAT3 (Figure 4G).

Transcriptomic Analysis of QD Treatment in LPS-Induced ALI Mice

The DESeq2 program was utilized for the detection of differentially expressed genes (DEGs) across groups, defining significance with FDR < 0.05 and $|\log2FC| \geq 1$. Between the LPS and control groups, 5105 DEGs were found, with 2796 upregulated and 2309 downregulated (Figure 5A). Comparing LPS+QD to LPS groups, 1067 DEGs were identified, with 347 upregulated and 720 downregulated (Figure 5B). Among 1067 DEGs related to ALI treatment, 315 were influenced by QD (Figure 5C). Clustering analysis using RSEM generated a heatmap showing gene expression differences across groups (Figure 5D). KEGG pathway analysis revealed 30 enriched pathways in the LPS + QD group relative to the LPS group, with a bubble chart highlighting the top 20 pathways (Figure 5E). Notably, the JAK/STAT signaling pathway was enriched, with JAK2 and STAT3 identified as key targets for QD. It underscores the potential importance of the JAK2/STAT3 pathway in the therapeutic effect of QD on ALI.

QD Inhibited the Activation of the JAK2/STAT3 Pathway in ALI Mice

Western blot analysis demonstrated that LPS-induced ALI mice had significantly increased phosphorylation of JAK2 and STAT3 proteins. However, this phosphorylation was notably inhibited by QD treatment. Additionally, the treatment with QD notably reduced the elevated levels of HIF-1α, IL-17A, and COX2 proteins within the pulmonary tissue of the mice (Figure 6).

QD Reduced LPS-Induced Inflammatory Response in RAW264.7 Cells and Inhibited the JAK2/STAT3 Signaling Pathway

In RAW264.7 cells, the CCK-8 assay showed that QD concentrations of 50 μg/mL, 100 μg/mL, and 200 μg/mL promoted cell proliferation, while concentrations above 400 μg/mL reduced it (Figure 7A). The RT-qPCR data revealed that QD

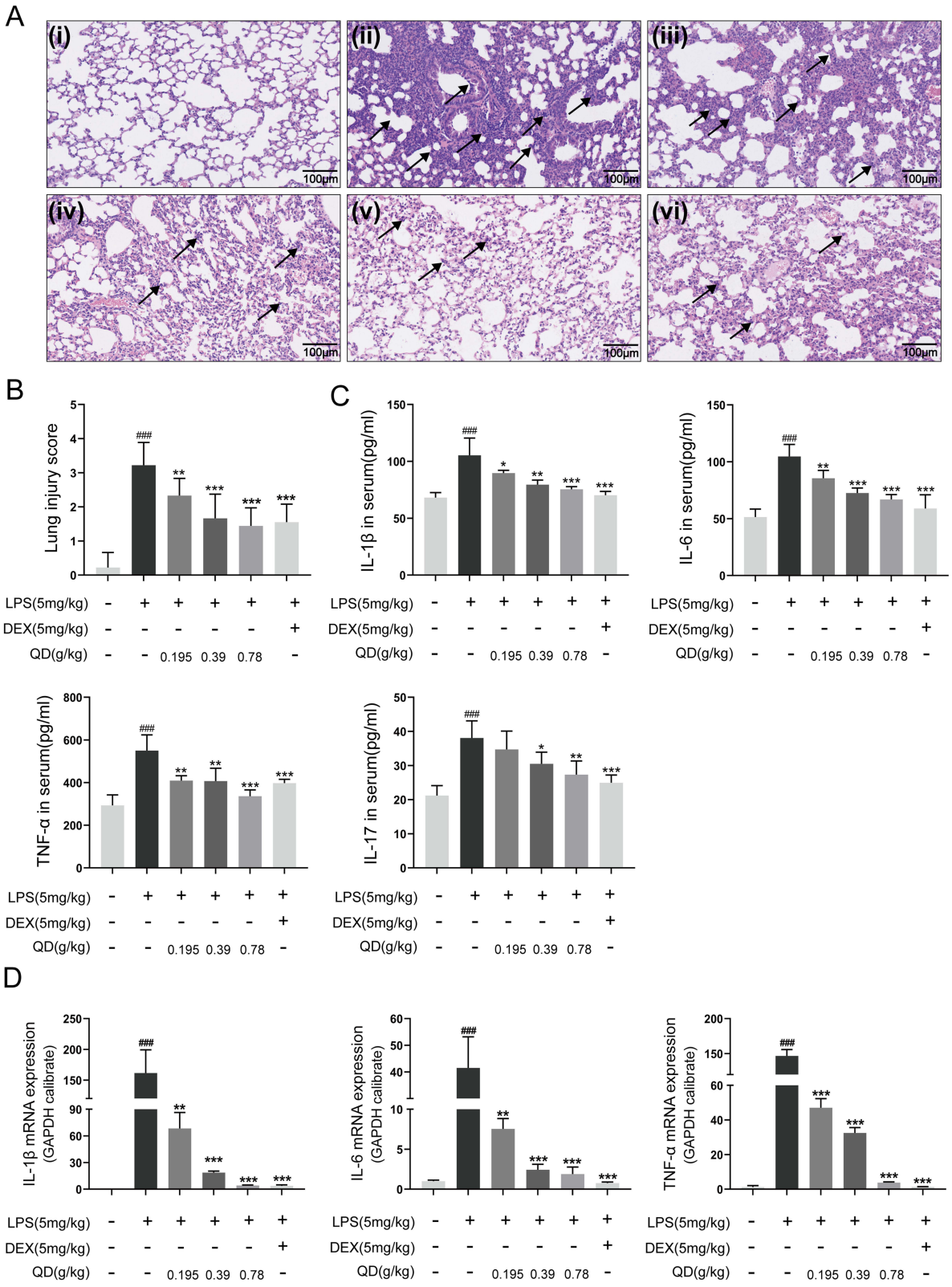

Figure 2 Qingdai (QD) alleviates inflammation in the pulmonary tissue of mice with ALI. Mice in the treatment groups were administered different doses of QD or dexamethasone (DEX) for 7 days; within one hour of the last gavage, the mice were intratracheally instilled with lipopolysaccharides (LPS) and euthanized 24 hours later. (**A**) Hematoxylin and Eosin staining (magnification: 200×; scale bar = 100 μm): (i) Control group, (ii) LPS group, (iii) QD-L (0.195 g/kg) group, (iv) QD-M (0.39 g/kg) group, (v) QD-H (0.78 g/kg) group, (vi) DEX group; the black arrows represent representative areas infiltrated by inflammatory cells. (**B**) Pathological scores of lung tissue. (**C**) The levels of IL-1β, IL-6, TNF-α, and IL-17 proteins in serum. (**D**) Relative mRNA expression levels of IL-1β, IL-6, and TNF-α in mouse lung tissue. Data are expressed as mean ± standard deviation (n=3). ### denote statistical significance at the 0.001 levels when compared to the control group, whereas *, **, and *** indicate significance at the 0.05, 0.01, and 0.001 levels, respectively, when compared to the LPS group.

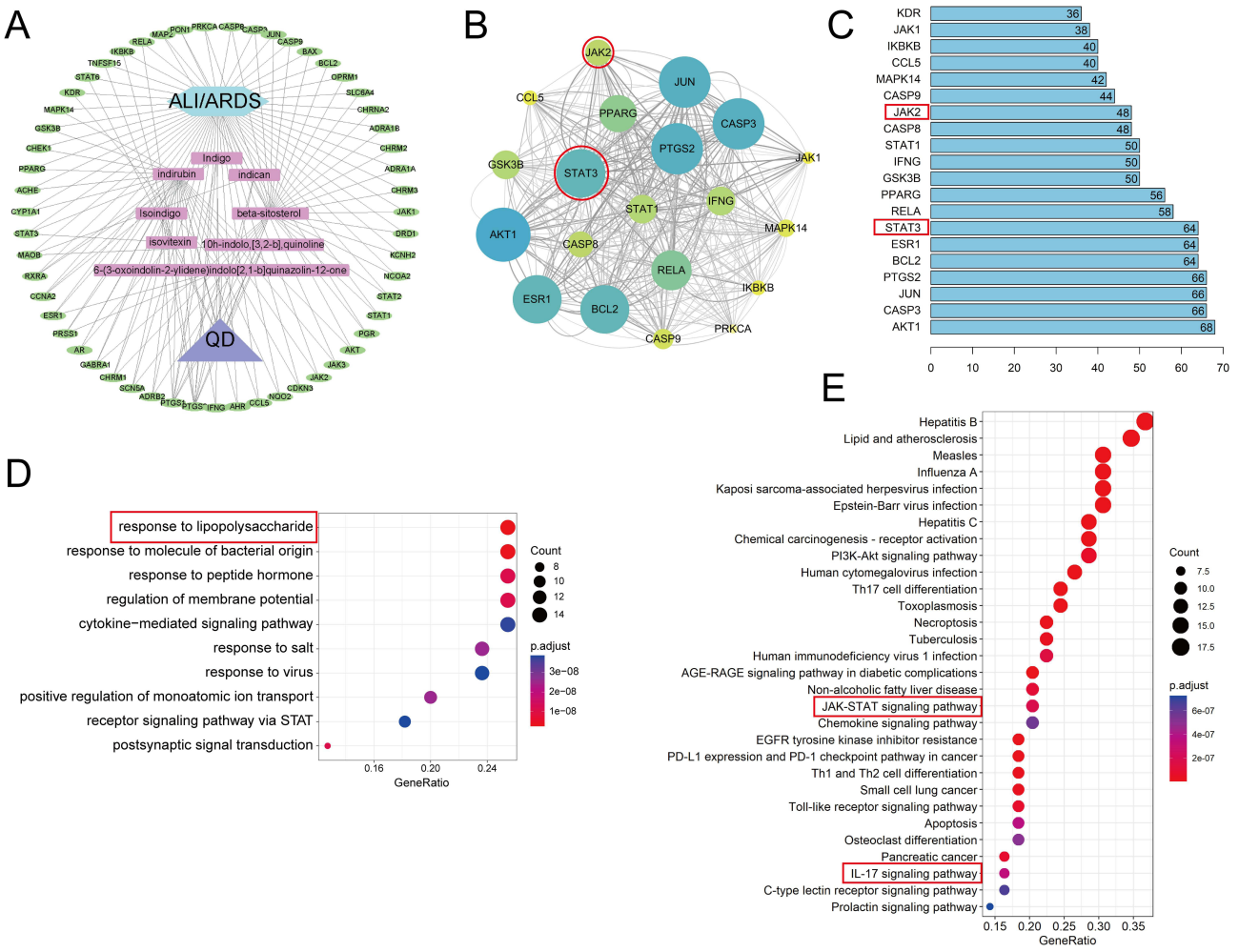

Figure 3 Network pharmacology prediction of potential targets and signaling pathways for Qingdai (QD) in treating ALI. (**A**) Disease-Compound-Target Pharmacological network: Blue represents the disease, blue-purple represents the drug name, light-red represents the active components of QD, and green represents disease targets. (**B**) The core PPI network is filtered from the network, containing the top 20 nodes ranked by degree. It consists of 20 nodes and 348 edges. Node color transitions from yellow to blue, indicating an increase in degree value, while larger node sizes represent higher degree values. (**C**) The top 20 target proteins ranked by degree value were identified using R software (R 4.2.2). (**D**) GO enrichment analysis of QD targets: In the bubble chart, larger dots indicate more genes in the entry, and redder colors represent higher enrichment levels. (**E**) KEGG enrichment analysis of QD targets: The lengths of the rectangles correspond to the gene count associated with each term, while the intensity of the red color signifies the level of enrichment.

markedly decreased the mRNA expression of IL-6, IL-1β, and TNF-α in cells stimulated by LPS. (Figure 7B). The ELISA data indicated that QD decreased the protein concentrations of IL-6, IL-1β, TNF-α, and IL-17 in the supernatants, showing a dose-dependent effect (Figure 7C). Western blot analysis revealed that QD effectively inhibited the elevated phosphorylation of JAK2 and STAT3 and reduced the expression of HIF-1α and IL-17A proteins (Figures 7D-7E).

Discussion

As a classical prescription, QD has been widely used to treat lung diseases in China for a long history due to its heat-clearing and detoxification effects. Previous studies have shown that QD can effectively alleviate ALI induced by influenza virus in mice[15] and its active component 2-Methylquinaozlin-4(3H)-one that has good antiviral activity.[23] In this study, the therapeutic effects and mechanisms of QD on ALI were systematically investigated by integrating high-resolution mass spectrometry, network pharmacology, transcriptomics, molecular docking, and validation experiments. First, UPLC-LTQ-Orbitrap-MS/MS identified indigo and indirubin as critical components of QD. Next, network pharmacology predicted 55 potential targets and found nine active ingredients with favorable oral bioavailability and drug-like properties. Subsequent PPI networks highlighted the hub targets such as AKT1, Caspase3, JAK1, STAT1,

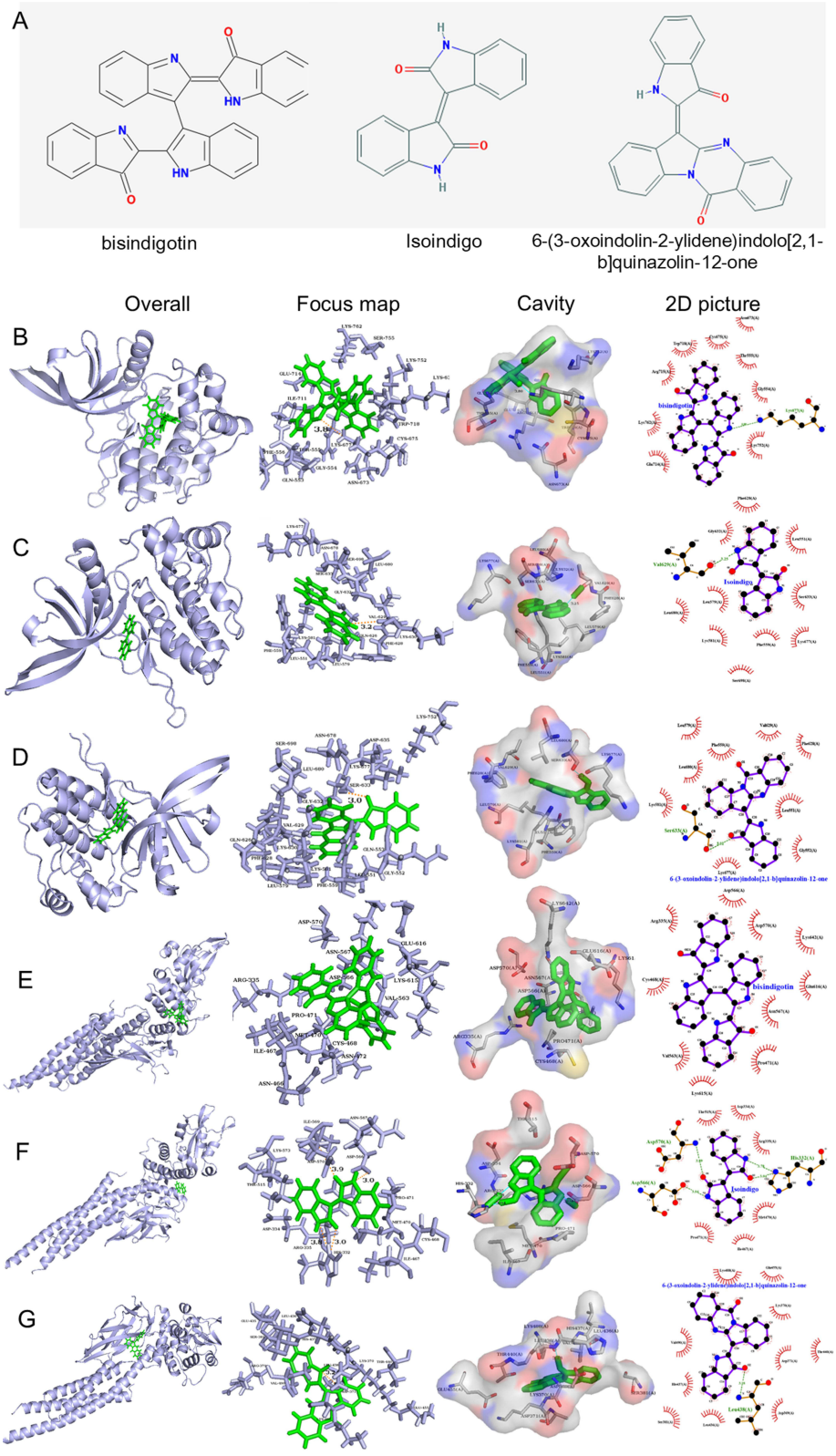

Figure 4 Molecular docking analysis. (**A**) The chemical structure of Bisindigotin, Isoindigo and 6-(3-oxoindolin-2-ylidene)indolo[2,1-b]quinazolin-12-one (IQO); (**B-D**) Molecular docking of bisindigotin with JAK2, Isoindigo with JAK2, IQO with JAK2; (**E-G**) Molecular docking of bisindigotin with STAT3, Isoindigo with STAT3, IQO with STAT3.

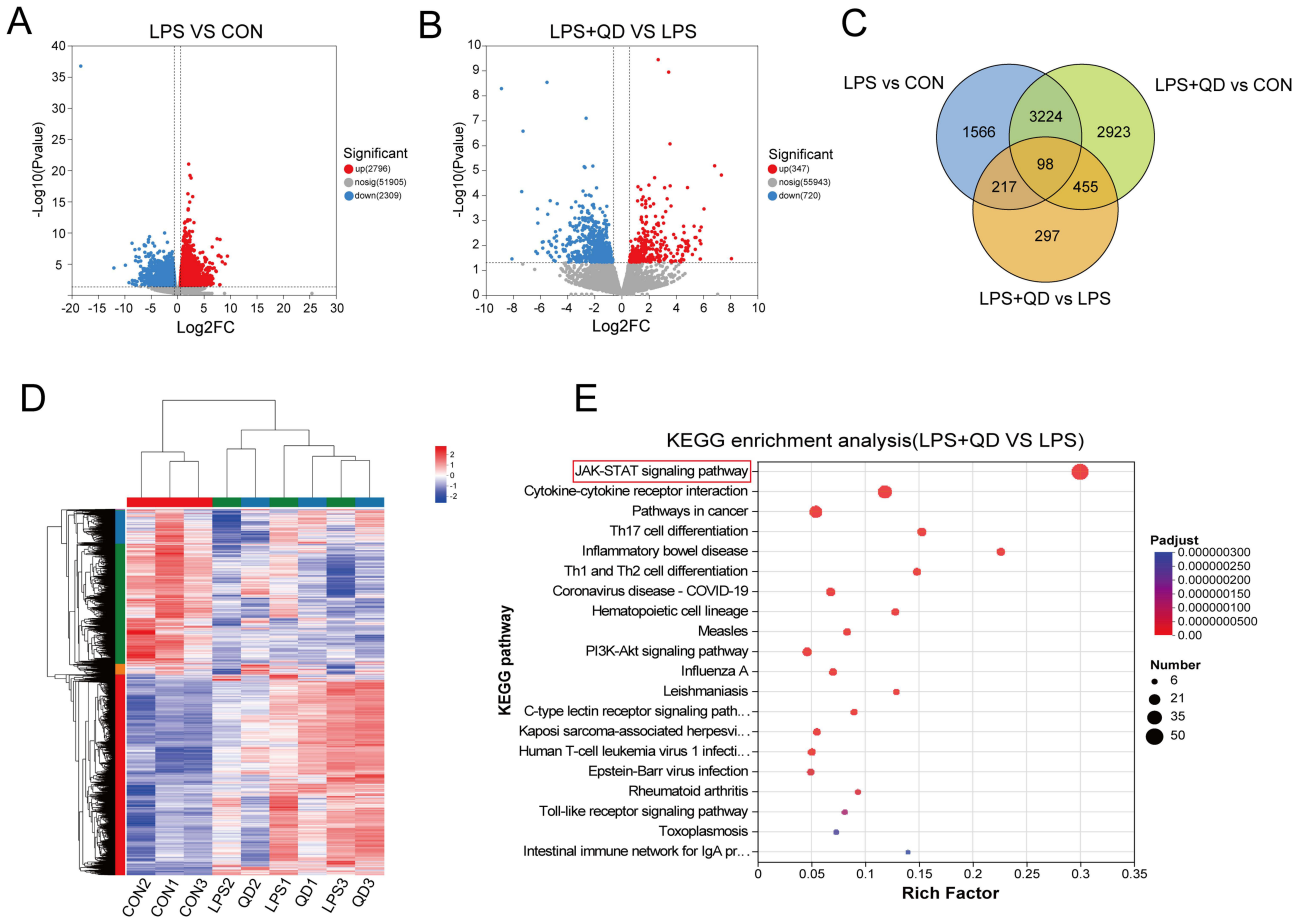

Figure 5 Transcriptomic analysis of lipopolysaccharides (LPS)-induced ALI mice treated with Qingdai (QD). (**A**) Volcano plot of differentially expressed genes (DEGs) between the LPS group and the control group; (**B**) Volcano plot of DEGs between the QD treatment group (LPS+QD) and the LPS group; (**C**) Venn diagram of DEGs; (**D**) Cluster analysis of DEGs. Red indicates higher gene expression in the sample, while blue indicates lower gene expression; (**E**) KEGG enrichment analysis. In the bubble chart, Dot sizes indicate the number of genes associated with each KEGG pathway, while the color indicates the range of adjusted p-values (Padjust).

JAK2, and STAT3. Then, functional enrichment showed QD impacts ALI by targeting processes related to LPS responses, while KEGG pathways underscored JAK/STAT and IL-17 signaling pathways.

Meanwhile, since the LPS-induced ALI mouse model mimics human pulmonary inflammation, showing alterations like alveolar hemorrhage, thickened alveolar walls, and inflammatory cell infiltration,[24] we explored the therapeutic mechanism of QD on this mode mouse. We found that QD significantly mitigated these inflammatory changes and lowered the levels of cytokines such as IL-1β, IL-6, TNF-α, and IL-17. Moreover, the transcriptomic analysis of lung tissue also enriched the JAK/STAT signaling pathway. Molecular docking identified bisindigotin, isoindigo, and IQO as potent QD components that disrupt JAK2 and STAT3 functions through specific interactions. Considering these findings, the JAK2/STAT3 pathway is proposed as a central mechanism for the efficacy of QD against ALI.

The JAK/STAT pathway is essential in ALI pathogenesis, affecting inflammation, apoptosis, and alveolar-capillary barrier integrity.[25,26] IL-6 is crucial in initiating inflammatory responses via the JAK2/STAT3 signaling pathway in cytokine storms.[27] STAT3 could interact with HIF-1α and act as a core to macrophage-driven inflammation through impacting IL-1β expression.[28,29] STAT3 could also affect the release of TGF-β and IL-17A.[30] IL-17, as a key inflammatory mediator, promotes the production of inflammatory factors like COX2 across various cell types.[31] In our validation experiments, QD demonstrated a decrease in the mRNA expression of IL-1β, IL-6, and TNF-α, as well as a suppression of protein expression for p-JAK2, p-STAT3, HIF-1α, IL-17A, and COX2 in the pulmonary tissue of LPS-induced ALI mice in a dose-dependent manner. These results confirm that QD could alleviate lung inflammation and tissue damage in LPS-induced ALI by inhibiting the JAK2/STAT3 signaling pathway.

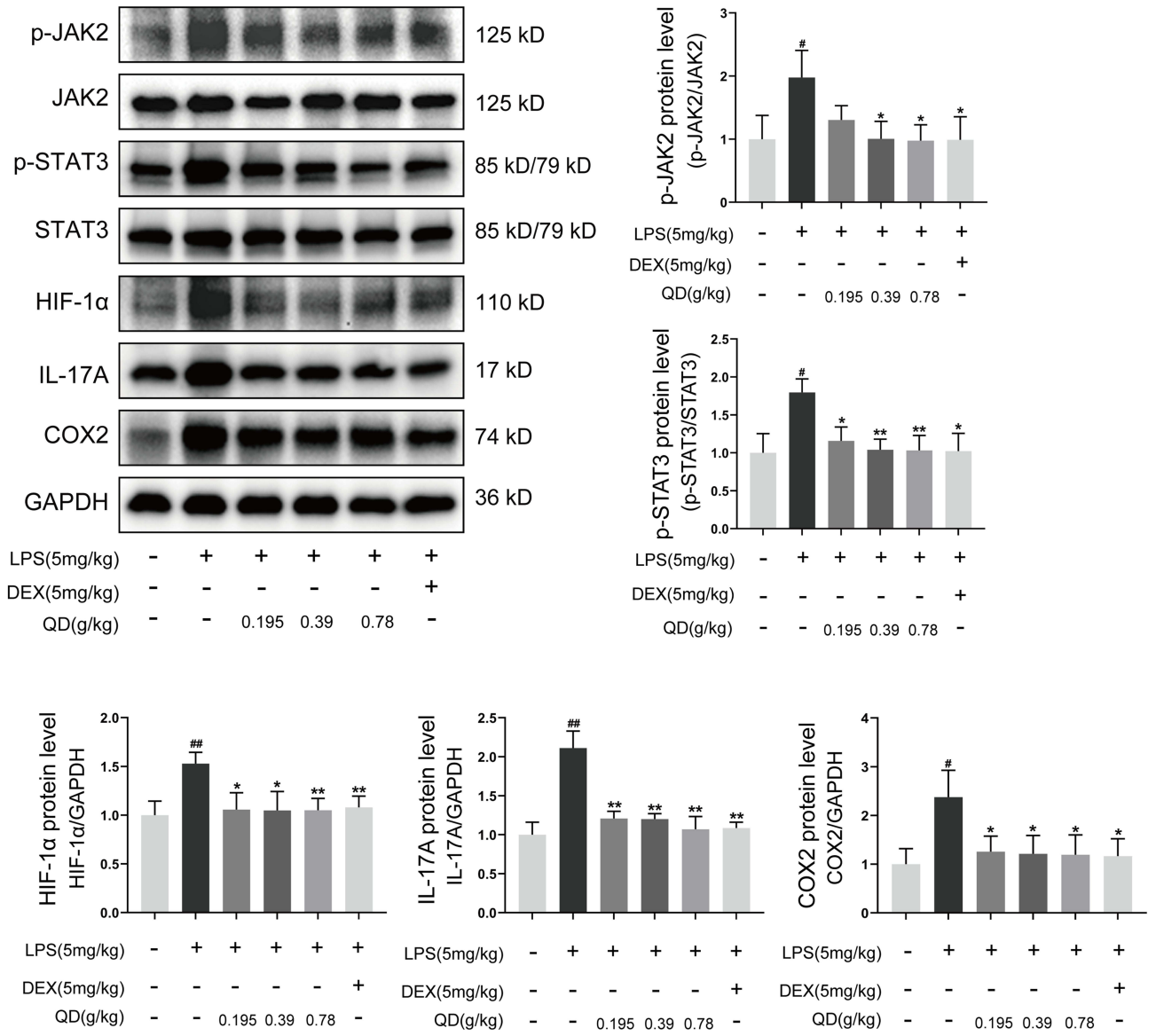

Figure 6 Qingdai (QD) suppressed the lipopolysaccharides (LPS)-induced JAK2/STAT3 signaling pathway in mice with ALI. Mice in the treatment groups were administered different doses of QD or dexamethasone for 7 days; within one hour of the last gavage, the mice were intratracheally instilled with LPS, and the lung tissues were collected 24 hours later. Protein expression levels of JAK2, p-JAK2, STAT3, p-STAT3, HIF-1α, IL-17A, and COX2 were analyzed by Western Blot. Data are expressed as mean ± standard deviation (n=3). # and ## denote statistical significance at the 0.05 and 0.01 levels, respectively, when compared to the control group, whereas * and ** indicate significance at the same levels when compared to the LPS group.

Macrophages are essential in innate immunity and can polarize into M1 or M2 phenotypes depending on stimuli. M1 macrophages emit proinflammatory cytokines such as IL-6, IL-1β, and TNF-α. Those cytokines are associated with pulmonary inflammation and cytokine release syndrome, which are the pivotal markers of severity in ALI.[32,33] The RAW264.7 cell line is a dependable system for investigating the activation and polarization of macrophages.[34] In the experiment, QD substantially alleviated the levels of IL-6, IL-1β, TNF-α, and IL-17 in RAW264.7 cells activated by LPS and additionally diminished the protein expression of p-JAK2, p-STAT3, HIF-1α, and IL-17A. These findings align with the results in vivo, suggesting that QD inhibits inflammatory responses in LPS-induced macrophages through the JAK2/STAT3 pathway.

Conclusion

In summary, the therapeutic effects of QD in ALI might be mediated by the modulation of the JAK2/STAT3 signaling pathway.

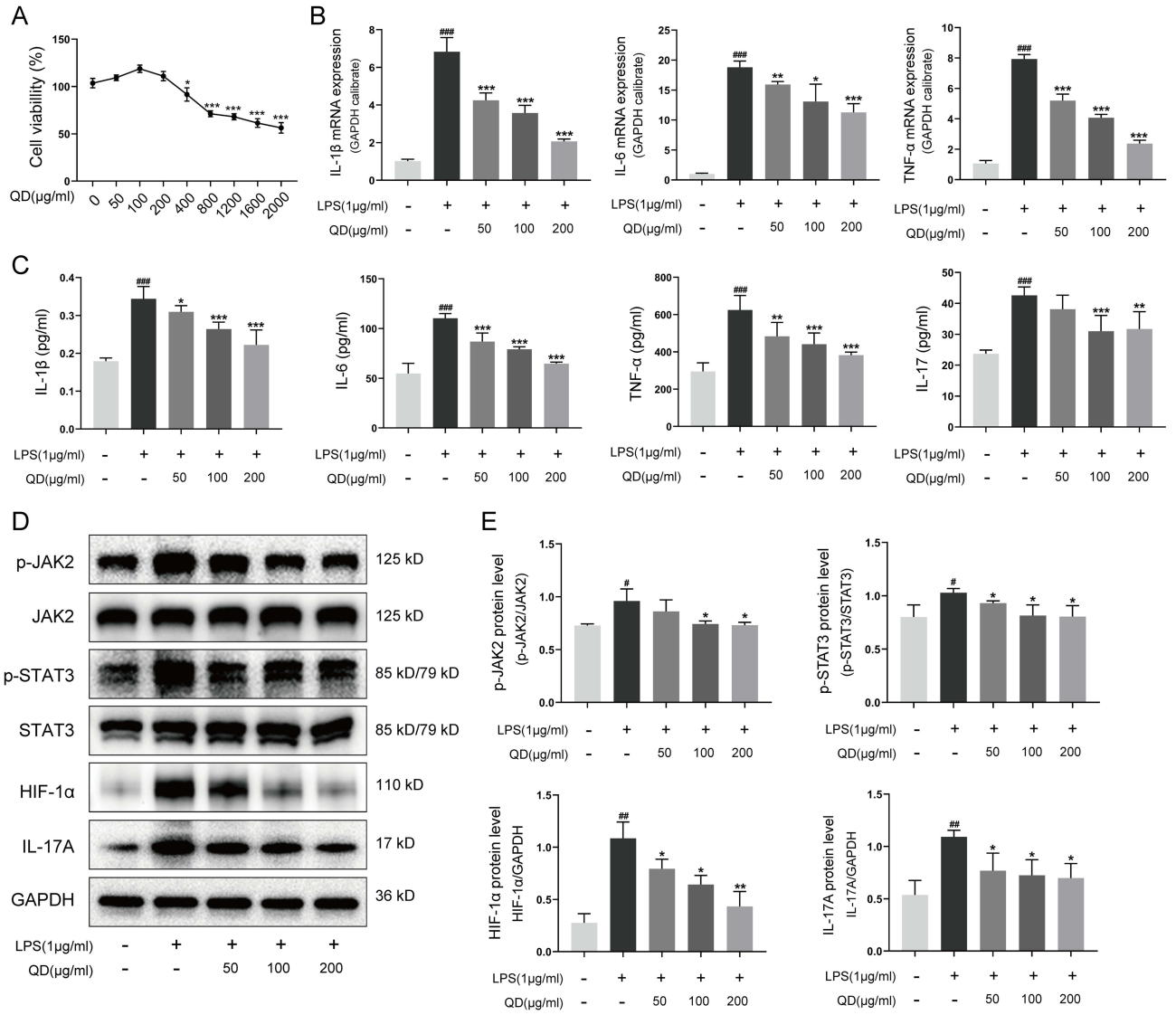

Figure 7 Qingdai (QD) reduced lipopolysaccharides (LPS)-induced inflammatory response in RAW264.7 cells and inhibited the JAK2/STAT3 signaling pathway. (**A**) Effect of QD on RAW264.7 cell viability. (**B**) QD reduced IL-6, IL-1β, and TNF-α mRNA expression in LPS-treated RAW264.7 cells. (**C**) QD reduced the protein expression of IL-6, IL-1β, TNF-α, and IL-17 in the supernatants of LPS-stimulated RAW264.7 cells. (**D-E**) QD inhibited the protein expression of p-JAK2, p-STAT3, HIF-1α, and IL-17A in LPS-induced RAW264.7 cells. Data are expressed as mean ± standard deviation (n=3). #, ##, and ### denote statistical significance at the 0.05, 0.01, and 0.001 levels, respectively, when compared to the control group, whereas *, **, and *** indicate significance at the same levels when compared to the LPS group.

Abbreviations

ALI, acute lung injury; COX-2, cyclooxygenase-2; DEX, dexamethasone; IL-1β, interleukin-1beta; IL-6, interleukin-6; IL-17, interleukin-17; IQO, 6-(3-oxoindolin-2-ylidene)indolo[2,1-b]quinazolin-12-one; JAK2, janus kinase 2; STAT3, signal transducers and activators of transcription 3; LPS, lipopolysaccharide; LTQ-Orbitrap-MS/MS, linear ion trap quadrupole-orbitrap mass spectrometry; MAPK, mitogen-activated protein kinase; QD, Qingdai; TCMSP, Traditional Chinese Medicine Systems Pharmacology Database and Analysis Platform; TCMID, Traditional Chinese Medicine Integrated Database; TNF, tumor necrosis factor; UPLC, ultra-high performance liquid chromatography.

Statement of Ethics

The animal experiment was approved by the Animal Ethics Committee of Shanghai University of Traditional Chinese Medicine (PZSHUTCM2310260005) and is consistent with the Experiments Guide for the Care and Use of Laboratory Animals. This study, which did not include experiments with human samples, is exempt from ethical review and approval

procedures according to items 1 and 2 of Article 32 of "the Measures for Ethical Review of Life Science and Medical Research Involving Human Subjects" in China.

This study only used data from a publicly available database, and ethical approval and informed consent were obtained from Yichang Central People's Hospital (2024-435-01).

Data Sharing Statement

The data is available upon request.

Funding

Fundings for this research were provided by Shanghai Municipal Science and Technology Major Project (No. ZXS004R4-1, No. ZD2021CY001), Natural Science Foundation project of Hubei Province (No. 2023AFB068), Medical and health project of Yichang Science and Technology Bureau (No. A23-1-022), Shanghai Shuguang Hospital Siming Project (No. SGXZ-201907), and Shanghai University of TCM Budget Project (No. 2021LK075).

Disclosure

The authors declare that there are no competing interests.

References

1. Zhou Y, Li P, Goodwin AJ. et al. Exosomes from endothelial progenitor cells improve outcomes of the lipopolysaccharide-induced acute lung injury. *Crit Care*. 2019;23(1):44. doi:10.1186/s13054-019-2339-3
2. Khemani RG, Smith L, Lopez-Fernandez YM, et al. Paediatric acute respiratory distress syndrome incidence and epidemiology (PARDIE): an international, observational study. *Lancet Respir Med*. 2019;7(2):115–128. doi:10.1016/S2213-2600(18)30344-8
3. Rubenfeld GD, Caldwell E, Peabody E, et al. Incidence and outcomes of acute lung injury. *N Engl J Med*. 2005;353(16):1685–1693. doi:10.1056/NEJMoa050333
4. Needham DM, Dinglas VD, Bienvenu OJ, et al. One year outcomes in patients with acute lung injury randomised to initial trophic or full enteral feeding: prospective follow-up of EDEN randomised trial. *BMJ*. 2013;346:1532. doi:10.1136/bmj.f1532
5. Wang J, Wu Q, Ding L, et al. Therapeutic effects and molecular mechanisms of bioactive compounds against respiratory diseases: traditional Chinese medicine theory and high-frequency use. *Front Pharmacol*. 2021;12:734450. doi:10.3389/fphar.2021.734450
6. Ding Z, Zhong R, Xia T, et al. Advances in research into the mechanisms of Chinese materia medica against acute lung injury. *Biomed Pharmacother*. 2020;122:109706. doi:10.1016/j.biopha.2019.109706
7. Chen S, Cheng Y. Case study of reducing sputum effect of Qingdai. *Mod Tradit Chin Med*. 2017;37(2):12–13. doi:10.13424/j.cnki.mtcm.2017.02.006 Chinese.
8. Ma J, Li J, Li Q, Cai Y, Sun S, Xu Y. Study on the medication patterns of modern famous traditional Chinese medicine master'diagnosis and treatment of lung flaccidity based on traditional Chinese medicine inheritance support system. *Mod Tradit Chin Med and Mater Medica-World Sci and Technol*. 2021;23(9):3126–3133.
9. Qi-Yue Y, Ting Z, Ya-Nan H, et al. From natural dye to herbal medicine: a systematic review of chemical constituents, pharmacological effects and clinical applications of indigo naturalis. *Chin Med*. 2020;15(1):127. doi:10.1186/s13020-020-00406-x
10. Zhang EX, Hao WW, Wang ZH, et al. Mechanism of action of Qingdai and its active ingredient Indigofera in regulating cellular pyroptosis in mice with ulcerative colitis through NF-κB signaling. *China J Tradit Chin Med Pharm*. 2023;38(10):4704–4710.
11. Gu SZ, XueY G, et al. Anti-inflammatory mechanism of QingDai in an inflammatory model of intestinal epithelial cells in ulcerative colitis. *Pharmacol Clin Chin Mater Med*. 2021;37(06):67–71. doi:10.13412/j.cnki.zyyl.2021.06.011 Chinese.
12. Yang QY, Ma LL, Zhang C, et al. Exploring the mechanism of indigo naturalis in the treatment of ulcerative colitis based on TLR4/MyD88/NF-κB signaling pathway and gut microbiota. *Front Pharmacol*. 2021;12:674416. doi:10.3389/fphar.2021.674416
13. Wang XL, Guo Z, Lin JM, et al. Indirubin protects chondrocytes and alleviates OA by inhibiting the MAPK and NF-KB pathways. *Int Immunopharmacol*. 2023;115:109624. doi:10.1016/j.intimp.2022.109624
14. Wang Q, Yu J, Hu Y, et al. Indirubin alleviates bleomycin-induced pulmonary fibrosis in mice by suppressing fibroblast to myofibroblast differentiation. *Biomed Pharmacother*. 2020;131:110715. doi:10.1016/j.biopha.2020.110715
15. Tu P, Tian R, Lu Y, et al. Beneficial effect of Indigo Naturalis on acute lung injury induced by influenza A virus. *Chin Med*. 2020;15(1):128. doi:10.1186/s13020-020-00415-w
16. Ru J, Li P, Wang J, et al. TCMSP: a database of systems pharmacology for drug discovery from herbal medicines. *J Cheminform*. 2014;6:13. doi:10.1186/1758-2946-6-13
17. Zhou BX, Li J, Liang XL, et al. beta-sitosterol ameliorates influenza A virus-induced proinflammatory response and acute lung injury in mice by disrupting the cross-talk between RIG-I and IFN/STAT signaling. *Acta Pharmacol Sin*. 2020;41(9):1178–1196. doi:10.1038/s41401-020-0403-9
18. Zhang Y, Qi Z, Wang W, et al. Isovitexin inhibits ginkgolic acids-induced inflammation through downregulating SHP2 activation. *Front Pharmacol*. 2021;12:630320. doi:10.3389/fphar.2021.630320
19. Huang JH, Huang XH, Chen ZY, et al. Dose conversion among different animals and healthy volunteers in pharmacological study. *Chin J Clin Pharmacol Ther*. 2004;9(09):1069–1072.
20. Dhlamini Q, Wang W, Feng G, et al. FGF1 alleviates LPS-induced acute lung injury via suppression of inflammation and oxidative stress. *Mol Med*. 2022;28(1):73. doi:10.1186/s10020-022-00502-8

21. Zhang J, Zhang M, Huo XK, et al. Macrophage inactivation by small molecule wedelolactone via targeting sEH for the treatment of LPS-induced acute lung injury. *Acs Central Sci*. 2023;9(3):440–456. doi:10.1021/acscentsci.2c01424
22. Li YC, Cao YM, Xiao J, et al. Inhibitor of apoptosis-stimulating protein of p53 inhibits ferroptosis and alleviates intestinal ischemia/reperfusion-induced acute lung injury. *Cell Death Differ*. 2020;27(9):2635–2650. doi:10.1038/s41418-020-0528-x
23. Tian R, Zhu HY, Lu Y, et al. Therapeutic potential of 2-methylquinazolin-4(3H)-one as an antiviral agent against influenza A virus-induced acute lung injury in mice. *Molecules*. 2022;27(22). doi:10.3390/molecules27227857
24. Kuhar E, Chander N, Stewart DJ, et al. A preclinical systematic review and meta-analysis assessing the effect of biological sex in lipopolysaccharide-induced acute lung injury. *Am J Physiol Lung Cell Mol Physiol*. 2024;326(6):L661–L671. doi:10.1152/ajplung.00336.2023
25. Abdul KH, Alhouayek M, Quetin-Leclercq J, Muccioli GG. 5'AMP-activated protein kinase: an emerging target of phytochemicals to treat chronic inflammatory diseases. *Crit Rev Food Sci Nutr*. 2024;64(14):4763–4788. doi:10.1080/10408398.2022.2145264
26. Xu R, Shao Z, Cao Q. MicroRNA-144-3p enhances LPS induced septic acute lung injury in mice through downregulating Caveolin-2. *Immunol Lett*. 2021;231:18–25. doi:10.1016/j.imlet.2020.12.015
27. Billing U, Jetka T, Nortmann L, et al. Robustness and information transfer within IL-6-induced JAK/STAT signalling. *Commun Biol*. 2019;2:27. doi:10.1038/s42003-018-0259-4
28. Scholz CC, Taylor CT. Targeting the HIF pathway in inflammation and immunity. *Curr Opin Pharmacol*. 2013;13(4):646–653. doi:10.1016/j.coph.2013.04.009
29. Fan Y, Dong W, Wang Y, et al. Glycyrrhetinic acid regulates impaired macrophage autophagic flux in the treatment of non-alcoholic fatty liver disease. *Front Immunol*. 2022;13:959495. doi:10.3389/fimmu.2022.959495
30. Zhong WJ, Liu T, Yang HH, et al. TREM-1 governs NLRP3 inflammasome activation of macrophages by firing up glycolysis in acute lung injury. *Int J Biol Sci*. 2023;19(1):242–257. doi:10.7150/ijbs.77304
31. El-Baz FK, Ali SI, Elgohary R, Salama A. Natural beta-carotene prevents acute lung injury induced by cyclophosphamide in mice. *PLoS One*. 2023;18(4):e0283779. doi:10.1371/journal.pone.0283779
32. Guan T, Zhou X, Zhou W, Lin H. Regulatory T cell and macrophage crosstalk in acute lung injury: future perspectives. *Cell Death Discov*. 2023;9(1):9. doi:10.1038/s41420-023-01310-7
33. Chua RL, Lukassen S, Trump S, et al. COVID-19 severity correlates with airway epithelium-immune cell interactions identified by single-cell analysis. *Nat Biotechnol*. 2020;38(8):970–979. doi:10.1038/s41587-020-0602-4
34. Khatua S, Simal-Gandara J, Acharya K. Understanding immune-modulatory efficacy in vitro. *Chem Biol Interact*. 2022;352:109776. doi:10.1016/j.cbi.2021.109776